Clim. Past, 5, 633–646, 2009
www.clim-past.net/5/633/2009/
© Author(s) 2009. This work is distributed under
the Creative Commons Attribution 3.0 License.

Climate of the Past

Antarctic ice-sheet response to atmospheric CO_2 and insolation in the Middle Miocene

P. M. Langebroek[1,*], **A. Paul**[1,2], **and M. Schulz**[1,2]

[1]Faculty of Geosciences, University of Bremen, Bremen, Germany
[2]MARUM – Center for Marine Environmental Sciences, University of Bremen, Bremen, Germany
[*]now at: Alfred Wegener Institute for Polar and Marine Research (AWI), Bremerhaven, Germany

Received: 17 July 2008 – Published in Clim. Past Discuss.: 12 August 2008
Revised: 15 September 2009 – Accepted: 18 September 2009 – Published: 22 October 2009

Abstract. Foraminiferal oxygen isotopes from deep-sea sediment cores suggest that a rapid expansion of the Antarctic ice sheet took place in the Middle Miocene around 13.9 million years ago. The origin for this transition is still not understood satisfactorily. One possible cause is a drop in the partial pressure of atmospheric carbon dioxide (pCO_2) in combination with orbital forcing. A complication is the large uncertainty in the magnitude and timing of the reconstructed pCO_2 variability and additionally the low temporal resolution of the available pCO_2 records in the Middle Miocene. We used an ice sheet-climate model of reduced complexity to assess variations in Antarctic ice sheet volume induced by pCO_2 and insolation forcing in the Middle Miocene. The ice-sheet sensitivity to atmospheric CO_2 was tested for several scenarios with constant pCO_2 forcing or a regular decrease in pCO_2. This showed that small, ephemeral ice sheets existed under relatively high atmospheric CO_2 conditions (between 640–900 ppm), whereas more stable, large ice sheets occurred when pCO_2 was less than ∼600 ppm. The main result of this study is that the pCO_2-level must have declined just before or during the period of oxygen-isotope increase, thereby crossing a pCO_2 glaciation threshold of around 615 ppm. After the decline, the exact timing of the Antarctic ice-sheet expansion depends also on the relative minimum in summer insolation at approximately 13.89 million years ago. Although the mechanisms described appear to be robust, the exact values of the pCO_2 thresholds are likely to be model-dependent.

1 Introduction

Over the last 65 million years (Ma) the climate of the Earth has undergone a long-term cooling (e.g. Zachos et al., 2001; Shevenell et al., 2004). Superimposed on this gradual cooling are several shifts of a sudden increase in oxygen isotope values ($\delta^{18}O$) and a global sea-level drop (Miller et al., 1998, 2005). These events indicate rapid cooling and expansion of the Antarctic ice sheet. The rapid transitions could be caused by changes in ocean circulation and closing/opening of gateways (e.g. Flower and Kennett, 1995), enhanced chemical weathering and burial of organic matter (e.g. Raymo, 1994), or low eccentricity forcing in combination with a decline in atmospheric CO_2 partial pressure (pCO_2) (Holbourn et al., 2005, 2007).

This study addresses the last hypothesis by exploring the response of the Antarctic ice sheet to variations in pCO_2 and insolation. The ice-sheet fluctuations of one of the most profound cooling events in the Cenozoic, the Middle Miocene climate transition (e.g. Shevenell et al., 2004; Holbourn et al., 2005) were computed in an ice sheet-climate model, which was forced by pCO_2 and insolation only. In the Middle Miocene the Antarctic continent was located close to its present position and the Antarctic Circumpolar Current was developed as well. Small, highly dynamic, ice sheets covered Antarctica in the Early Miocene (e.g. Pekar and DeConto, 2006; Van Tuyll et al., 2007) and possibly started expanding from ∼15 Ma in an orbitally-paced fashion (Shevenell et al., 2008). We investigated the final advance into a large ice sheet, which occurred between 13.9 and 13.8 Ma (Holbourn et al., 2005). High-resolution benthic $\delta^{18}O_c$ records (Shevenell et al., 2004; Holbourn et al., 2005) show a mean increase of approximately 0.5‰ for this transition (Fig. 1).

A remarkable difference of this glaciation with respect to earlier events (e.g. the Eocene-Oligocene transition, DeConto and Pollard, 2003; Coxall et al., 2005; Pollard and DeConto, 2005) is the relatively small decline in atmospheric CO_2 content. From the Early Miocene onwards, pCO_2 values were relatively low and fluctuations small (e.g. Zachos et al., 2008, and references therein). Unfortunately, the set of published pCO_2 data covering the Middle Miocene is

Correspondence to: P. M. Langebroek
(petra.langebroek@awi.de)

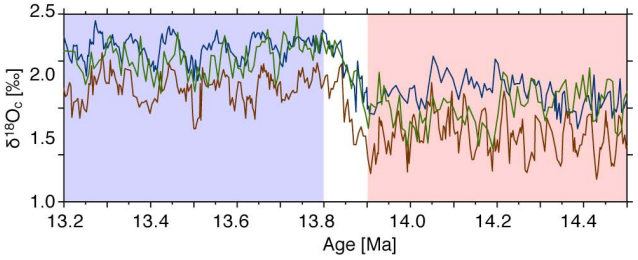

Fig. 1. Compilation of high-resolution benthic $\delta^{18}O_c$ records for the Middle Miocene. The two records from Holbourn et al. (2005) are plotted in blue (Site 1237) and red (Site 1146). Another ODP record (Site 1171), at latitudes closer to Antarctica, is indicated in green (Shevenell et al., 2004) on the same time scale. The mean difference for every record from the period before (13.9–14.5 Ma) to after (13.2–13.8 Ma) the transition is approximately 0.5‰.

very small. The methods used to reconstruct paleo-pCO_2 levels (e.g. alkenones, Pagani et al., 2005, stomatal index, Kürschner et al., 2008, and boron isotopes, Pearson and Palmer, 2000; Demicco et al., 2003) involve large uncertainties. Furthermore, the different methods result in values that differ by more than 100–200 ppm amongst each other, indicating even larger errors than those assigned to the individual reconstructions.

We first explore the stability of the modeled Antarctic ice sheet under a large range of pCO_2 levels in order to determine pCO_2-thresholds for which the Antarctic continent glaciates and deglaciates (hysteresis experiments). Secondly, the ice-sheet response to variations in insolation is investigated by keeping the pCO_2 at a constant level. Thirdly, the combined effect of varying pCO_2 and insolation forcings on the ice-sheet size are assessed.

2 Methods and experimental set-up

2.1 Ice sheet-climate model

In this study, we used a coupled ice sheet-climate model. The ice-sheet component has previously been applied to study Quaternary Northern Hemisphere glaciations (Sima, 2005; Sima et al., 2006). We changed the model set-up to an Antarctic configuration, forced only by pCO_2 and insolation. Furthermore we extended the model by including important climatic feedbacks.

The climate component consists of three large-scale boxes covering the entire southern hemisphere: a low (0–30° S), middle (30–60° S) and high (60–90° S) latitude box (Fig. 2). The forcing consists of seasonal orbital forcing based on Laskar et al. (2004) combined with prescribed atmospheric pCO_2 levels. In the large-scale boxes of the climate model, energy is conserved and redistributed by meridional energy transport, taking into account the latent heat fluxes due to

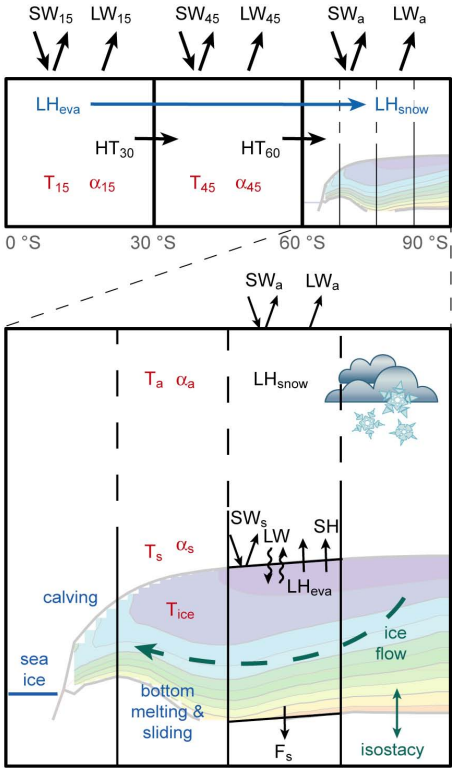

Fig. 2. Set-up of the model. Upper: Large-scale box model consisting of low (0–30° S), middle (30–60° S) and high (60–90° S) latitude cells. Each compartment is forced by shortwave (SW) and longwave (LW) radiation at the top of the atmosphere and sensible heat transport by eddies (HT), as well as latent heat transport induced by evaporation and snowfall (LH). The two lower latitude boxes are described by one general temperature (T) and albedo (α). Lower: The high-latitude, Antarctic box is subdivided into smaller grid cells with a resolution of 0.5° in latitude. For each cell the energy and mass balances are solved for surface and atmospheric temperatures (T_s and T_a, respectively). Fluxes include incoming and outgoing shortwave radiation at the top of atmosphere (SW_a) and at the land/ice/snow surface (SW_s); reflected longwave radiation at the top of atmosphere (LW_a); longwave (LW), sensible heat (SH) and latent heat of evaporation (LH_{eva}) fluxes between the surface and atmosphere; latent heat of snowfall in atmosphere (LH_{snow}); heat flux into underlying bedrock (F_s). In all boxes ice flow velocities and ice height are computed, depending on the mass balance, local temperature (T), albedo (α) and isostasy.

evaporation and snow accumulation. The physical processes within the high latitude box are resolved in 0.5° latitude bands. In these boxes, energy balances of the atmosphere and surface are resolved separately, but computed simultaneously. Additionally, the mass balance for the ice-sheet component is modeled. Daily computation is necessary, because the orbital cycle as well as processes of snow accumulation and melting have a strong seasonal imprint (Pollard, 1983).

The atmospheric and surface energy balances include parameterizations for short- and long-wave radiation, latent heat of evaporation and snowfall, sensible heat exchange, heat flux into the surface and energy used by melting of ice and snow (Pollard, 1982, 1983; Jentsch, 1987, 1991; Wang and Mysak, 2000). Total snow accumulation and its latitudinal distribution is tuned to the present-day (total) Antarctic accumulation. The parameterization for snowfall depends on surface temperature, distance from the coast, surface height and daily surface temperature (Oerlemans, 2002, 2004). Therefore, it includes important processes such as the elevation-desert effect (Pollard, 1983).

The ice-sheet model is symmetric around the South Pole. Within the ice sheet, flow velocities and temperatures are computed with a vertical resolution of 12 layers. The altitude and ice thickness of every latitude grid cell are derived by solving the continuity equation using basal melting, local bedrock isostasy and a surface mass balance (Sima, 2005; Sima et al., 2006). The initial ice-free bedrock topography is reconstructed using the BEDMAP project database (Lythe et al., 2000) for bedrock elevation and ice thickness, considering local isostasy. For the axially symmetric ice-sheet model, the high spatial resolution of the dataset is reduced, averaging the topography into the 0.5° wide latitude bands. The initial bedrock used by the model is a simplified version of the zonally-averaged topography that includes a bulge close to the continental shelf and a flatter hinterland, resembling East Antarctica. Although no separate ocean component is included in the model, the energy and mass balances within the Antarctic box include the albedo of (seasonally varying) sea-ice. This is parameterized depending on the near-surface temperature of the appropriate grid cells. The surface albedo of the Antarctic continent depends on the ice and snow content of the corresponding grid cell and combines albedos of land (0.3), ice (0.35) and snow (0.75). A more detailed description of the climate forcing can be found in the Appendix.

2.2 Climate sensitivity of the model

The equilibrium climate sensitivity as estimated from 19 different atmospheric general circulation models ranges from 2.1 to 4.4°C, with an average of 3.2°C (Randall et al., 2007). These models do not include a dynamic ice-sheet component, but do account for changes in snow cover and albedo. To tune the climate sensitivity of our model, we first ran the coupled ice sheet-climate model for the last 100 ka with constant pre-industrial pCO_2 of 280 ppm and varying orbital parameters. The modeled present-day ice sheet is in equilibrium with the radiative forcing and has a volume of 25.0×10^{15} m^3, similar to its estimated present-day size (e.g. Huybrechts et al., 2000; Oerlemans, 2002; Huybrechts, 2004). The mean hemispheric surface temperature is 14.9°C. We deliberately enhanced the model sensitivity to changes in pCO_2 in order to account for the missing water vapor feedback (see Appendix). In the tuned model, a doubling of pCO_2 while maintaining fixed ice-sheet height and (seasonal) insolation distribution results in a hemispheric mean temperature increase of 2.5°C. This value falls within the range of the values reported by the IPCC report (2007). The largest increase is found in atmospheric and surface temperatures in the Antarctic high latitude box, with values up to 3.9 and 4.4°C, respectively. This polar amplification is due to the included ice-albedo feedback and is comparable to pCO_2-doubling simulations in comprehensive climate models (e.g. Masson-Delmotte et al., 2006a,b).

2.3 Insolation and pCO_2 forcings

Based on Earth's orbital elements as computed by Laskar et al. (2004) we calculated daily insolation (Berger, 1978a,b) at the top of the atmosphere (for every latitude box) and at the surface for the high resolution Antarctic cells (60–90° S). We used two different averages for comparison to ice-volume variations: annual mean and caloric summer (half-year of highest values) insolation. Since the atmospheric CO_2 level in the Middle Miocene is not very well constrained, the model was forced by prescribed scenarios of constant pCO_2 and by a constant decrease in pCO_2.

2.4 Experimental set-up

Firstly, hysteresis experiments were carried out in order to find pCO_2-threshold values at which the Antarctic continent (de)glaciates. Two experiments were performed, one with and one without orbital forcing. The former started at 35 Ma at a pCO_2 level of 1120 ppm. After slowly decreasing pCO_2 to 280 ppm (reached at 20 Ma), pCO_2 was increased again to 1400 ppm (at 0 Ma). Because of this very slow decrease, the timing of the orbital parameters is not very important and the results would be similar if the experiments had started earlier or later. The latter experiment followed a similar scheme, but started with 560 ppm at 20 Ma. pCO_2 of 280 ppm was reached at 15 Ma and was increased to 1120 ppm at 0 Ma. In this case the timing is irrelevant, because the orbital parameters were fixed to present-day. In both experiments, the rate of pCO_2 decrease as well as increase was 280 ppm/5 Ma (as in Pollard and DeConto, 2005) and ice volume is considered to be close to equilibrium.

Secondly, different levels of constant atmospheric CO_2 were applied for model runs of a 1 Ma period, from 14.2 to 13.2 Ma (preceded by a 100 ka long spin-up time). This allows investigation of the effect of insolation fluctuations on ice-sheet volume under different constant pCO_2 conditions. The range between 300 and 1100 ppm was investigated in steps of 50 ppm with an increased resolution of 10 ppm from 590 to 650 ppm.

Thirdly, sensitivity experiments involving a reduction in pCO_2 were carried out, focusing on ice-sheet response to the level, rate and timing of pCO_2 decrease. These experiments

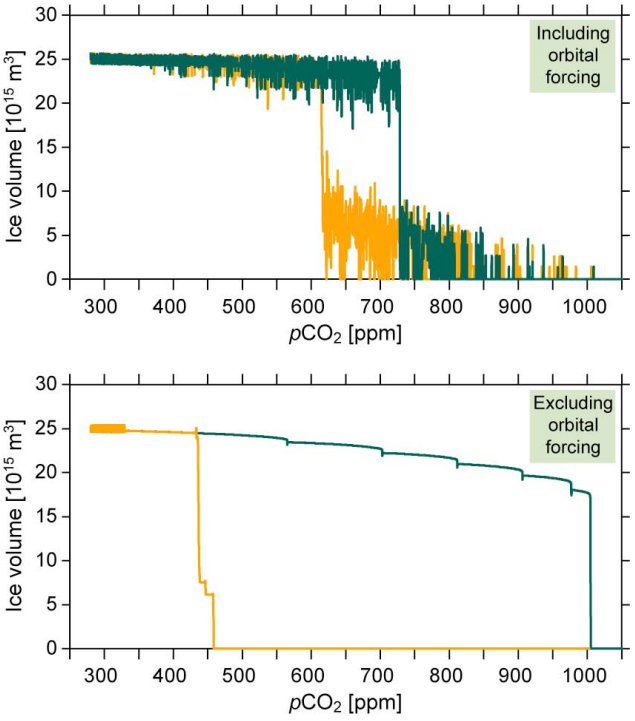

Fig. 3. Hysteresis experiment. Starting from no-ice conditions and high pCO_2 (orange) or starting from full ice sheet and low pCO_2 (green). Upper panel shows hysteresis including orbital forcing, lower panel without orbital variations. Rate of pCO_2 change is 280 ppm/5 Ma.

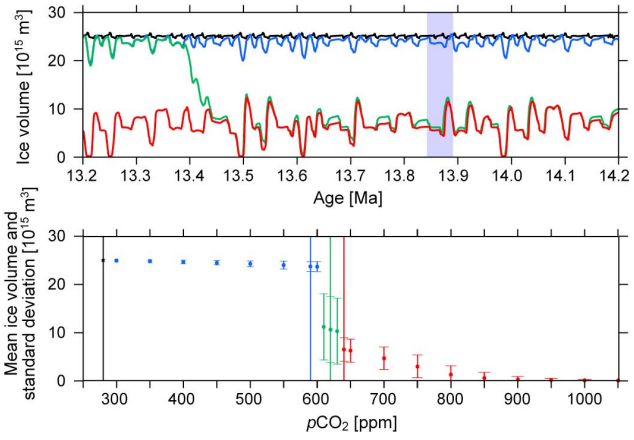

Fig. 4. Constant pCO_2 experiments in the Middle Miocene (14.2–13.2 Ma). Upper: Resulting ice-volume variations of four typical pCO_2 forcing (280 ppm (black), 590 ppm (blue), 620 ppm (green) and 640 ppm (red)). Lower: Mean ice volume (dot) and standard deviation (arrows) of large (black/blue) and small (red) ice sheets, defined by their pCO_2 level. The blue rectangle shows the Middle Miocene glaciation period as indicated by oxygen-isotope records.

ran from 14.1 to 13.7 Ma (without spin-up time) with varying insolation.

In all experiments daily insolation as a function of latitude was applied. The computations were performed at a daily time-step.

3 Results

3.1 Hysteresis experiments

To assess the sensitivity of the simulated ice volume to pCO_2 changes and to find the critical range of pCO_2 at which the Antarctic continent (de)glaciates, two types of hysteresis experiments were performed. The first included orbital variations, whereas the second was only forced by atmospheric CO_2 (Fig. 3). In the former case of including orbital variations, the (rapid) transition into a large ice sheet occurred around 615 ppm, preceded by a semi-stable small ice sheet. Orbital forcing acts as noise, therefore the ice sheet deglaciated under a relatively low pCO_2 when this was included (∼725 ppm), resulting in a small hysteresis window of approximately 110 ppm. In the latter case, where the orbital variations were omitted, glaciation and deglaciation occurs at ∼436 and 1004 ppm, respectively, accounting for a much larger hysteresis window of ∼568 ppm. The modeled rate of pCO_2 change was slow at 280 ppm/5 Ma, similar to the experiments of Pollard and DeConto (2005).

3.2 Constant pCO_2 experiments

The critical pCO_2 for glaciation is around 615 ppm, when including orbital forcing. Below this threshold the entire Antarctic continent glaciates, with mean ice volumes between 23 and 25×10^{15} m^3 (Fig. 4). Between ∼640 and ∼700 ppm small ice sheets exist (almost) continuously over the entire modeled period. Higher pCO_2 levels result in small, ephemeral ice sheets. Under constant pCO_2 forcing and insolation derived from Middle Miocene orbital parameters (between 14.2 and 13.2 Ma) either large or small ice sheets occurs (Figs. 4 and 5). Only constant pCO_2 values close to the threshold of 615 ppm cause a transition between these two states. Using constant 620 ppm forcing, Antarctica glaciates at 13.43 Ma.

The small ice sheets show large variations in ice volume, up to $\sim2.3\times10^{15}$ m^3 for constant pCO_2 of 640 ppm. The volume of large ice sheets vary less under constant pCO_2 conditions, with a maximum standard deviation of $\sim1.0\times10^{15}$ m^3 for pCO_2 values close to the threshold and nearly no variance at lower pCO_2 levels. Two runs with constant pCO_2 close to the glaciation threshold and maximum ice-volume variability are used to represent the large ice sheet (590 ppm) and the small ice sheet (640 ppm).

The correlation between ice-volume variation and annual and summer mean insolation was computed for every 5°

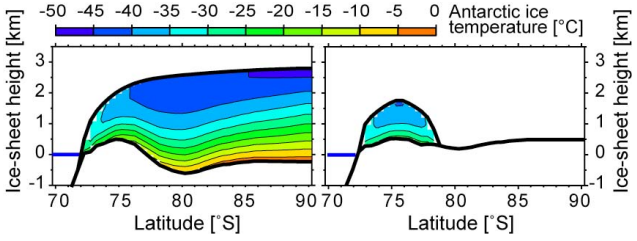

Fig. 5. Cross-section of large (left) and small (right) Antarctic ice sheets. Color scale corresponds to annual mean ice temperatures.

of southern latitude (Fig. 6). Variations in volume of both the large and small ice sheet correlate better to high (maximum around 70° S), than to low latitudes. In the case of the large ice sheet, the highest correlation coefficients are reached when ice volume lags insolation by approximately 2 ka. Maximum correlation coefficient values are 0.28 and 0.78 for annual and summer mean insolation, respectively. The small ice sheet matches insolation averages best for a lag of 5–6 ka. Maximum correlation coefficients for annual and summer mean insolation are 0.49 and 0.62, respectively.

3.3 Varying pCO_2 experiments

The first sensitivity test focusses on initial and final pCO_2 levels. In this set of experiments atmospheric CO_2 decreases linearly at a rate of 50 ppm/ka (Fig. 7 – yellow to red curves). In every experiment, the mid-point of the pCO_2 drop occurs at the same moment in time (13.9 Ma), varying only the initial and final pCO_2 levels. The resulting ice volume transitions occur at about the same time, whereby the largest difference in pCO_2 forces the most rapid ice-sheet transition (Fig. 7 – red curve). Repeating the experiment for different slopes of the pCO_2 transition gives practically identical results (not shown).

The second test investigates the effect of the rate at which the atmospheric CO_2 decreases during ice-sheet growth (Fig. 7 – blue curves). Experiments forced by a slow decrease in pCO_2 result in a variable duration of ice-sheet transition, between 20–30 ka. In runs with a rapid pCO_2 drop, the transition length is independent of the pCO_2 drawdown rate. This relation also holds for different timings of the pCO_2-transition (not shown).

In the last set of sensitivity experiments, the forcing is applied at different moments in time resulting in different timing of the ice-sheet expansion (Fig. 8).

4 Discussion

4.1 Hysteresis experiments

In the hysteresis experiment including Miocene orbital variations, a glaciation pCO_2-threshold of approximately

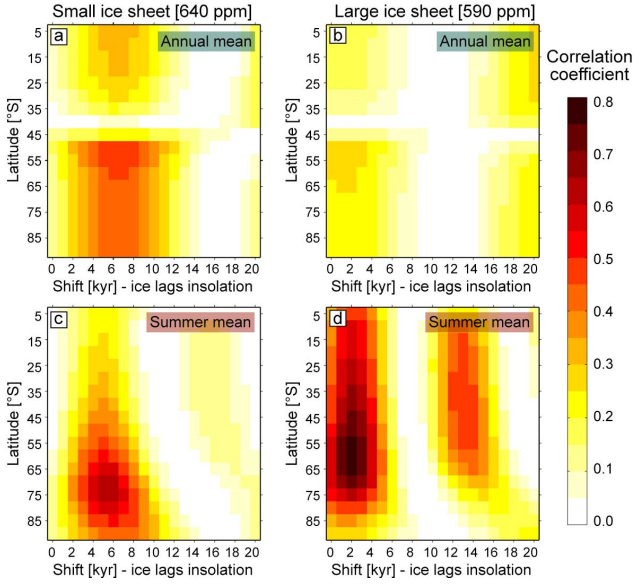

Fig. 6. Ice-sheet variations correlated to insolation at latitudes between 0 and 90° S. Insolation is shifted backwards in time by 1 ka on horizontal axis (ice volume lags insolation). Correlation coefficients are given for a small (**a** and **c**) and large (**b** and **d**) ice sheet and for annual (a and b) and summer mean (c and d) insolation. Best correlation is found for latitudes around 70° S and a shift of 5–6 ka (small ice sheet) or 2 ka (large ice sheet). Highest correlation coefficients for a small ice sheet are 0.49 and 0.62, for annual and summer mean insolation, respectively. Maxima for a large ice sheet are 0.28 (annual) and 0.78 (summer mean insolation).

615 ppm is found. The Antarctic ice sheet deglaciates when the pCO_2 increases by another ∼110 ppm (at ∼725 ppm). Annual mean temperatures over Antarctica differ by approximately 2.5°C between the glaciation and deglaciation thresholds. This hysteresis window is slightly smaller than in simulations with the ice-sheet model of Pollard and DeConto (2005) (∼120 ppm), but similar to the computations of Huybrechts (1993). The latter author proposed a range in hysteresis width varying between ∼1 and 5°C depending on the initial bedrock topography. Using a present-day orbital setting, Antarctic glaciation and deglaciation occurs under ∼435 and ∼1005 ppm, respectively (Fig. 3). This much larger hysteresis window is consistent with the findings of Pollard and DeConto (2005). Nevertheless, the synthetic set of orbital parameters applied by DeConto and Pollard (2003) and Pollard and DeConto (2005) resulted in a less extreme insolation variation than the orbital parameters used in this study (following Laskar et al., 2004). Indeed, when applying the DeConto and Pollard (2003) set of orbital parameters the hysteresis window increases to approximately 140 ppm (not shown).

Unlike the width of the hysteresis window, the threshold values differ from previous studies (Huybrechts, 1993;

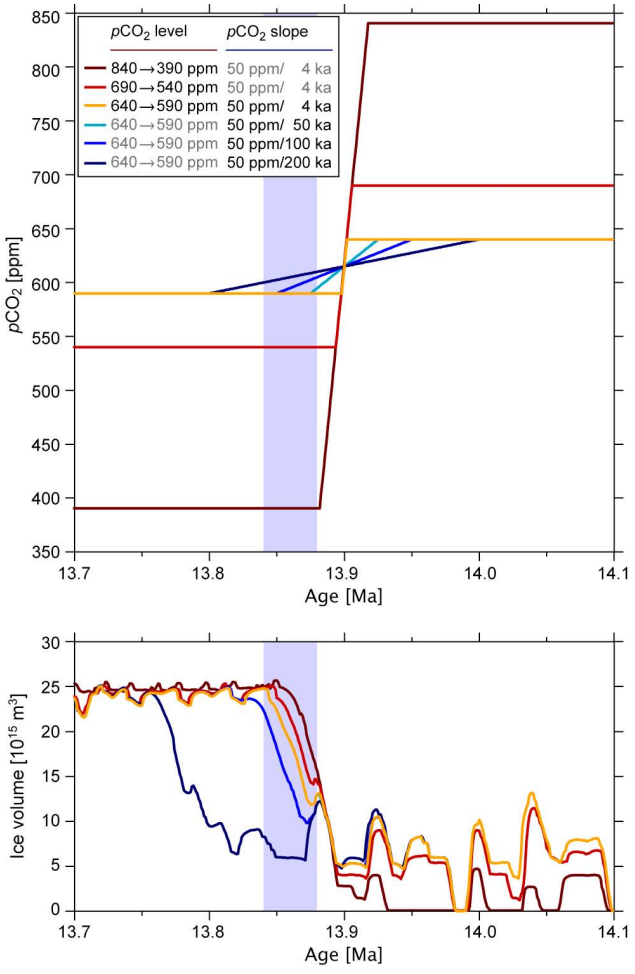

Fig. 7. pCO_2 sensitivity experiments – level of initial and final pCO_2 (yellow to red colors) and rate of pCO_2 decrease (blue colors). Colors in upper panel show pCO_2 forcing and correspond to ice-volume transition in lower panel. Blue box indicates approximate Antarctic glaciation as retrieved from sedimentary records. Glaciation is independent from initial and final pCO_2 levels (red to orange). On the contrary, the rate of the pCO_2 drawdown is important. Extremely slow drop in pCO_2 (dark blue) results in delayed ice-sheet extension, relatively slow decrease (light blue) causes appropriate timing with glaciation. A pCO_2 drop of 50 ppm/50 ka or faster (for example 50 ppm/4 ka in orange) gives the same ice-sheet transition as 50 ppm/50 ka.

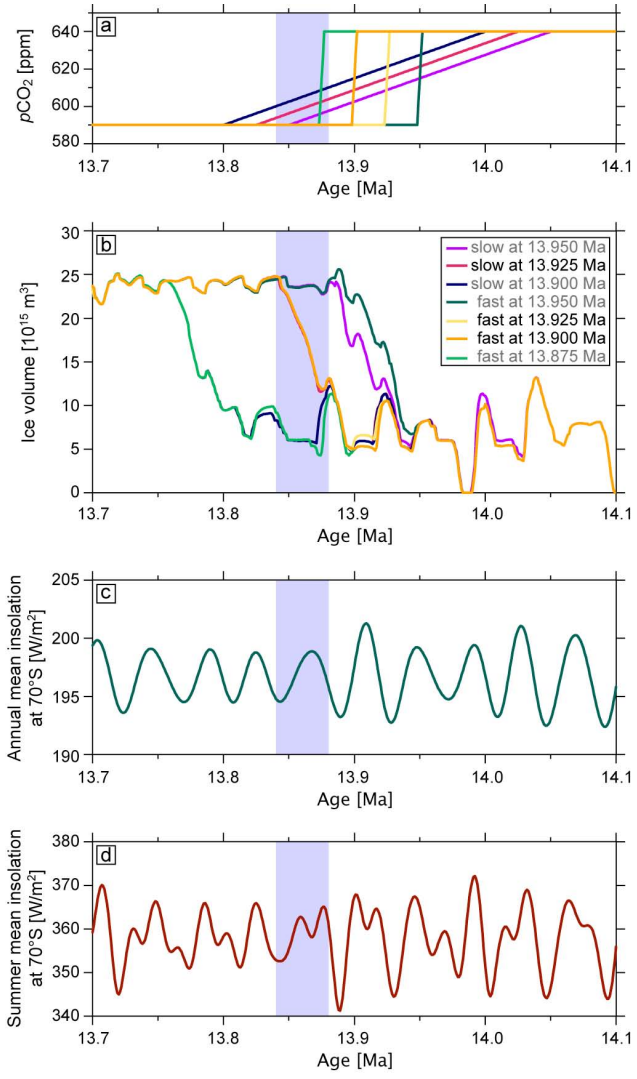

Fig. 8. pCO_2 sensitivity experiment – timing of pCO_2 decrease. Colors in **(a)** show pCO_2 forcing and correspond to ice-volume transition in **(b)**. Blue box indicates approximate Antarctic glaciation as found in sedimentary records. Green/orange curves result from fast pCO_2 transition (50 ppm/4 ka); purple/blue ones from a slow drop (50 ppm/200 ka). Black (gray) text in legend indicates best (not) fitting solutions (see Discussion section). Orange and dark blue curves correspond to their counterparts in Fig. 7. **(c)** Annual mean insolation at 70° S. **(d)** Summer mean insolation at 70° S.

Pollard and DeConto, 2005). These show glaciation and deglaciation thresholds under much higher Antarctic temperatures (10–20°C higher than present-day, Huybrechts, 1993) or higher pCO_2 levels (∼780 and ∼900 ppm, DeConto and Pollard, 2003). Although the values of DeConto and Pollard (2003) and DeConto et al. (2008) apply well to the Eocene-Oligocene transition, it is unlikely that pCO_2 levels in the Middle Miocene declined from values above ∼780 ppm. The relatively low glaciation threshold modeled in this study is much closer to the pCO_2-reconstructions for the Middle Miocene (e.g. Pearson and Palmer, 2000; Demicco et al., 2003; Pagani et al., 2005; Kürschner et al., 2008).

We repeated the experiments for a higher value of the CO_2-emission factor (see Sect. A4 in the Appendix) in the Southern high-latitude box. This implies a stronger polar amplification, and indeed higher annual mean Antarctic temperatures were computed (maxima of ∼11.6°C). The

resulting hysteresis window shifted to lower pCO_2-values, with a glaciation threshold of approximately 400 ppm and a deglaciation around 425 ppm.

The modeled glaciation threshold value also depends on the initial bedrock topography. Huybrechts (1993) showed that the difference in Antarctic mean temperature between a flat and an unloaded present-day bedrock topography is approximately 8°C, with higher bedrock elevations glaciating at higher temperatures. The initial bedrock topography used in this study has elevations in between these extreme bedrock scenarios. Increasing the initial topography would probably cause an Antarctic glaciation under higher pCO_2-values. The exact effects should be investigated in a bedrock-sensitivity study, which is beyond the scope of this study.

Another modeled process possibly affecting the glaciation threshold is the mass balance computation. The ice sheet-climate model lacks an interactive hydrological model. The total accumulation and its latitudinal distribution is tuned to values describing the present-day Antarctic ice sheet and depends on distance to the South Pole, surface height and daily surface temperature. However, if other factors have a large impact on the local mass balance and were significantly different in the past, the glaciation threshold might be different.

In summary, the pCO_2 threshold values could be slightly different than presented above, mainly depending on the initial bedrock topography. If the climate sensitivity and the hydrological cycle were significantly different in the past, these would also affect the threshold values.

4.2 Constant pCO_2 experiments

Two types of stable ice sheets occur under the large range of pCO_2-levels investigated (Fig. 4). Small ice sheets show large ice-volume variations, where obliquity and precession are the dominant frequencies. On the other hand, large ice sheets reveal smaller ice-volume variations. These small fluctuations have a stronger influence of precession over obliquity and are therefore stronger correlated to summer insolation than to annual mean insolation (Fig. 6). Huybers and Tziperman (2008) found a comparable relation between the ice-sheet size and the dominant frequencies for a Northern Hemisphere Pliocene ice sheet. They proposed that in the warm climate conditions under which thin (small) ice sheets occur, a long ablation season can counterbalance the opposite effect precession has on summer and fall insolation. The higher insolation intensity is then counteracted by a shorter summer duration. This effect reduces the precession signal in the ice-volume variations, and the obliquity becomes the dominant frequency. Raymo and Niscancioglu (2003) proposed that the obliquity signal is the result of variations in the insolation gradient between low and high latitudes, causing variations in the meridional moisture and heat fluxes. However, our results show a strong obliquity frequency in the ice volume without explicitly calculating a moisture flux between low and high latitudes. Our modeled obliquity could be caused by the opposing effects of insolation intensity and duration (as proposed by Huybers and Tziperman, 2008), because we included daily insolation in the ice sheet-climate model. In large ice sheets the ablation period is too short to be influenced by this effect.

The difference in time lag between ice volume and insolation (5–6 ka for a large ice sheet versus 2 ka for a small ice sheet) is probably also related to the different frequencies dominating the ice-volume variations. Large ice sheets appear to be closer to resonance with the precessional forcing and therefore show a small time lag. Small ice sheets follow precessional forcing less closely, which explains the large time lag to insolation forcing.

The Antarctic ice-sheet expansion largely depends on a strong minimum in (summer) insolation (see next section), indicating a dependence on the insolation intensity, not on the summer duration.

Under constant pCO_2, the small ice sheets show much larger variations in volume than the large ice sheets. This can partly be observed in the oxygen-isotope record (Table 1). An F-test shows that the variance of the original oxygen-isotope data in the restricted time domains is significantly different (significance level of 90%). This difference might be explained by the fact that small ice sheets are more easily perturbed by changes in the forcing. Additionally, ablation plays a major role in ice-volume variations and occurs on two sides of the small ice sheet, whereas the large ice sheet only has an ablation zone at the outer rim (Fig. 5).

Correlations between continental ice volume and the oxygen isotopic composition of seawater vary around 1‰ for 100 m sea-level change (e.g. Fairbanks and Matthews, 1978; Schrag et al., 1996; Zachos et al., 2001). Using the present ocean area (3.6×10^6 km^2) and the densities of water and ice (1000 kg/m^3 and 910 kg/m^3, respectively), an apparent sea-level drop of 100 m is equivalent to ice build-up with a volume of approximately 40×10^{15} m^3. The ice-volume variations in the large and small ice sheet result in sea-level fluctuations of 2.654 and 6.840 m, respectively (Table 1). This corresponds to δ^{18}O variations of 0.027 and 0.068‰. Accordingly, the fluctuations in the modeled ice-volume records can explain ∼17 and ∼36% of the variations found in the benthic oxygen-isotope records. The calibration does not account for variations in pCO_2 and does not take care of any effects caused by changes in (deep sea) temperature, salinity, local runoff, oxygen-isotope ratio of the ice, etc. Notwithstanding the crude calibration, the correlation between the standard deviations of data- and model-derived oxygen-isotope ratios is high.

The synchronous eccentricity and obliquity minima at ∼13.84 Ma (Abels et al., 2005) result in a relatively constant, average-to-low insolation. This has been proposed as being partly responsible for the large-scale glaciation in the Middle Miocene (Holbourn et al., 2005). In our ice sheet-climate model, the occurrence of such a special configuration or natural variability in insolation itself is not sufficient

Table 1. Standard deviation of benthic oxygen-isotope records (cf. Shevenell et al., 2004; Holbourn et al., 2005) compared to the standard deviation derived from the modeled ice volume of the example constant pCO_2 experiments. Typical large ice sheet exists under 590 ppm (Fig. 5 – left); typical small ice sheet is found under a constant pCO_2 of 640 ppm (Fig. 5 – right).

Time interval [Ma]	13.2–13.8	13.9–14.5	References and comments
Standard deviation $\delta^{18}O$ [‰]	0.160	0.207	Site 1146 (Holbourn et al., 2005)
Standard deviation $\delta^{18}O$ [‰]	0.127	0.159	Site 1237 (Holbourn et al., 2005)
Standard deviation $\delta^{18}O$ [‰]	0.172	0.202	Site 1171 (Shevenell et al., 2004)
Mean of above standard deviations [‰]	**0.153**	**0.189**	for comparison to modeled ice-volume fluctuations
pCO_2 [ppm]	590	640	
Mean ice volume [10^{15} m^3]	23.7	6.5	Modeled results; Examples of the
Standard deviation ice volume [10^{15} m^3]	1.051	2.710	ice-sheet shape can be found in
Apparent sea level [m]	2.654	6.840	Fig. 5 – for a large (left) and
Derived $\delta^{18}O$ [‰]	**0.027**	**0.068**	a small (right) ice sheet
Percentage of data explained [%]	**17**	**36**	

for an Antarctic glaciation at that time. Only constant atmospheric CO_2 levels at or very close to the threshold of 615 ppm can induce a transition from small to large ice volume (Fig. 4). However, the modeled timing of the transition occurs ∼450 ka later than the transition identified from oxygen isotope records. Therefore, in order to glaciate the Antarctic continent at the right moment in time, a decrease in pCO_2 seems unavoidable (as previously proposed by Holbourn et al., 2005).

All high-resolution oxygen-isotope records (Shevenell et al., 2004; Holbourn et al., 2005) show a mean increase of approximately 0.5‰ from the period before (13.9–14.5 Ma) to the period after (13.2–13.8 Ma) the rapid transition (see also Fig. 1). The two stable large and small ice-sheet simulations around the pCO_2-threshold have average ice volumes of ∼23.7 and $\sim 6.5\times10^{15}$ m^3. A pCO_2-decline between these two states would result in a sea level difference of ∼43.3 m. This sea-level drop would increase the oxygen-isotope ratio of sea water by approximately 0.43‰. This suggests that more than 85% of the Middle Miocene oxygen-isotope transition found in the sedimentary records can be explained by ice-volume expansion on Antarctica. In future research this comparison will be further investigated by including oxygen isotopes directly in the ice sheet-climate model.

4.3 Varying pCO_2 experiments

The first sensitivity test (see Sect. 3.3) showed that a larger difference between initial and final pCO_2 forcing resulted in a faster ice-sheet expansion. This can be explained by the different variability of the ice sheet at different pCO_2 levels. The larger standard deviations of 1.051×10^{15} m^3 and 2.710×10^{15} m^3 (Table 1) in the 590 and 640 ppm runs, respectively, increase the probability for insolation variations to act against a rapid ice-volume transition. The sedimentary records do not indicate such a rapid glaciation (e.g. Shevenell et al., 2004; Holbourn et al., 2005), but do show large variability in time (Fig. 1). Furthermore, under high pCO_2 levels hardly any ice covered the Antarctic continent (Fig. 4 and 7). Previous studies (e.g. Pekar and DeConto, 2006) did show evidence for a dynamic ice sheet shortly before the Middle Miocene. Therefore, the relatively small difference in pCO_2 between 640 and 590 ppm, crossing the threshold value of ∼615 ppm, was used in the remaining sensitivity experiments.

The second sensitivity test dealt with the slope of the atmospheric CO_2 drawdown (Fig. 7 – blue curves). The duration of the ice-sheet transition was defined as the period in which ice volume is larger than the maximum volume of the small ice sheet and smaller than the minimum size of the large ice sheet. Additional experiments showed that the slow forcing did not have a strong effect on the duration of the ice-sheet expansion. The duration merely depended on the timing of the pCO_2 drop. This quite constrained timing (see next paragraph) limited the glaciation event to a length of approximately 30 ka, comparable to the time interval of 30–40 ka derived from $\delta^{18}O$ records (cf. Holbourn et al., 2005).

The third set of sensitivity experiments investigated the timing of the pCO_2 decrease for 50 ppm/200 ka and for 50 ppm/4 ka (Fig. 8). The best fit to $\delta^{18}O$ data (glaciation time shown by blue box) occurred when the simulations crossed the pCO_2 threshold of approximately 615 ppm between ∼13.90 and ∼13.93 Ma.

It has been proposed that the final step in Antarctic glaciation occurs due to synchronous minima in eccentricity and obliquity around 13.84 Ma (e.g. Holbourn et al., 2005; Abels et al., 2005), which resulted in average to low summer and annual mean insolation at 70° S. Also in our ice sheet-climate model, the abrupt large-scale ice-volume increases occur

during minima in summer insolation. For a modeled ice-sheet expansion to occur in the Middle Miocene at the same time as indicated by the shift to heavier benthic oxygen-isotope ratios in the sedimentary records, the minimum in high-latitude summer insolation at approximately 13.89 Ma appears to be the most suitable candidate for triggering the transition. A clear example is the experiment of fast pCO_2 decrease at 13.925 Ma (Fig. 8 – yellow curve), where an increasing insolation opposed ice growth. Only when the summer insolation reached the minimum of ∼13.89 Ma, the ice volume expanded. Our results suggest 13.89 Ma as a more important insolation moment for the Antarctic glaciation than the previously suggested 13.84 Ma. These experiments were based on a 50 ppm difference in pCO_2, but extending this range would give similar results (see first sensitivity test).

The comparison of the three sensitivity experiments to high-resolution oxygen-isotope records indicates that pCO_2 should drop below the threshold of ∼615 ppm just before the ice-sheet transition (as suggested by Holbourn et al., 2005). Most probably the initial and final pCO_2 levels were close to the threshold values, otherwise the variation in the ice-sheet volume was extremely small or even no ice was covering the Antarctic continent. The exact timing of the ice-sheet expansion depends largely on the orbital parameters, where the minimum of summer and annual mean insolation at ∼13.89 Ma takes a key position.

5 Conclusions

Despite the relatively simple geometry of our ice sheet-climate model, the realistically tuned climate sensitivity and hysteresis experiments allows us to conclude that the mechanism described below is robust. However, exact values are model dependent and should only be taken as a guideline.

1. It is very unlikely that a constant pCO_2 in combination with orbital forcing induced the large-scale Antarctic glaciation in the Middle Miocene. Constant levels produced either a large (below ∼610 ppm) or a small (above ∼630 ppm) ice sheet. Modeled ice volume had a smaller ice-volume standard deviation than expected from benthic oxygen-isotope records. The residual variation in these isotope records probably originate from fluctuations in pCO_2 and other changes in climatic or local conditions.

2. The extent of the pCO_2 drawdown was not important for the timing or duration of the glaciation transition, as long as it crossed the ∼615 ppm threshold. Moderate or quick pCO_2 reductions resulted in comparable and realistic ice-sheet extension. The timing of the pCO_2 decrease was important, because favorable orbital parameters enhanced the ice-sheet expansion. In order to expand the Antarctic ice sheet in the appropriate time interval as indicated by benthic oxygen-isotope records (13.84–13.88 Ma) the pCO_2 threshold must have been crossed between ∼13.90 and ∼13.93 Ma.

3. After the decrease in pCO_2 the minimum in summer insolation restricted the timing of ice growth on Antarctica. Therefore, the main ice-sheet expansion probably started around 13.89 Ma.

Appendix A

Model description

The ice sheet-climate model is controlled by energy and mass balances. Orbital elements are derived following the work of Laskar et al. (2004). They drive the seasonal solar radiation at the top of the atmosphere and define, together with the pCO_2, the amount of energy entering the entire climate system.

A1 Energy and temperature balances

The model consists of three large-scale boxes covering the entire southern hemisphere: a low (0–30° S), middle (30–60° S) and high (60–90° S) latitude box (Fig. 2). Within the climate system energy is conserved and changes in time are described by (Pollard, 1983; Hartmann, 1994):

$$\frac{\partial E_{\mathrm{ao}}}{\partial t} = R_{\mathrm{TOA}} - \Delta F_{\mathrm{ao}} + LH \tag{A1}$$

where E_{ao} is the total energy in the system, t the time, R_{TOA} the net incoming solar radiation at the top of the atmosphere, ΔF_{ao} the divergence of the meridional energy transport in the ocean as well as in the atmosphere, and LH the latent heat added to the atmosphere after condensation and freezing of water vapor. The net incoming radiation is the sum of the incoming short-wave radiation (SW_p) and the outgoing short- and long-wave radiation (LW_p):

$$R_{\mathrm{TOA}} = SW_p^{\downarrow} - SW_p^{\uparrow} - LW_p^{\uparrow}.$$

Radiation fluxes in the two *lower latitude* boxes (0–30° S and 30–60° S) are parameterized as:

$$SW_p^{\downarrow} - SW_p^{\uparrow} = Q(1-\alpha_p)$$

$$LW_p^{\uparrow} = \varepsilon_p \sigma T_a^4 + f_{\mathrm{CO_2}}$$

where Q is the solar insolation at the top of the atmosphere, α_p the planetary albedo, ε_p the planetary emissivity and σ the Stefan-Boltzmann constant. T_a is interpreted as the near-surface air temperature and $f_{\mathrm{CO_2}}$ as the effect of the atmospheric CO_2 content (cf., Myhre et al., 1998):

$$f_{\mathrm{CO_2}} = -8\frac{\ln(\frac{\mathrm{CO_2}}{280})}{\ln(2)} \approx 2.8 - 0.7\ln(\mathrm{CO_2}).$$

Therefore, a doubling of pCO_2 from 280 ppm (pre-industrial conditions) to 560 ppm accounts for a reduction of 8 W/m^2 in the outgoing longwave radiation of the two lower latitude boxes, accounting not only for pCO_2, but also for other greenhouse gases (mainly water vapor, see Sect. A4).

The physical processes in the *high latitude* box are deciphered in much higher resolution and complexity. For every 0.5° latitude energy and mass balances for the atmosphere and for the surfaces are simultaneously solved. Atmospheric temperature (T_a) is described by:

$$C_a \frac{dT_a}{dt} = R_a + LW + SH + LH_{\text{eva}} + LH_{\text{snow}}$$

and surface temperature (T_s) by:

$$C_s \frac{dT_s}{dt} = R_s - LW - SH - LH_{\text{eva}} - F_s - F_m$$

where $C_{a,s}$ is the heat capacity for the atmosphere and surface, respectively.

The incoming energy at the top of the atmosphere and at the surface is represented as (Jentsch, 1987; Wang and Mysak, 2000):

$$\begin{aligned} R_a &= SW_a^{\downarrow} - SW_a^{\uparrow} - LW_a^{\uparrow} \\ &= Q(1-\alpha_a)(1-\tau)(1+\tau\alpha_s) - (\varepsilon_2 \sigma T_a^4 + (1-\varepsilon_1)\sigma T_s^4) \end{aligned}$$

$$\begin{aligned} R_s &= SW_s^{\downarrow} - SW_s^{\uparrow} \\ &= \tau Q(1-\alpha_a)(1-\alpha_s) \end{aligned}$$

where τ is the atmospheric transmissivity of solar radiation, $\alpha_{a,s}$ the atmospheric and surface albedos, ε_2 an emissivity constant and ε_1 a term describing the greenhouse effect (see below).

The longwave and sensible heat fluxes between the atmosphere and surface are parameterized as:

$$LW = \sigma T_s^4 - \varepsilon_1 \sigma T_a^4$$

$$SH = \lambda(T_s - T_a)$$

where λ is a heat exchange coefficient which in principle depends on wind speed, atmospheric density and heat capacity, but is taken to be constant. The heat flux into the subsurface soil or upper ice layer (F_s) is given by:

$$F_s = \frac{2k_1}{\Delta z_1}(T_s - T_a)$$

where k_1 is the thermal conductance of snow and Δz_1 the depth range of conduction.

The latent heat due to evaporation (LH_{eva}) is parameterized as (Hartmann, 1994):

$$LH_{\text{eva}} = \rho_{\text{air}} L_v C_{\text{DE}} U [q_s^*(1-\text{RH}) + \frac{\text{RH}}{B_e}\frac{c_p}{L_v}(T_s - T_a)]$$

where ρ_{air} is the air density, L_v is the latent heat of vaporation, C_{DE} an exchange coefficient, U the wind speed, q_s^* the sea surface humidity, B_e the equilibrium Bowen ratio, c_p the specific heat of dry air and RH the relative humidity.

The latent heat associated with snowfall (LH_{snow}) depends on the accumulation of snow:

$$LH_{\text{snow}} = L_s A$$

where L_s is the latent heat of sublimation and A the accumulation. The snow is considered to be evaporated in the low latitude box, accounting for the LH-term in the energy equation (Eq. A1). The total accumulation and its latitudinal distribution is tuned to the present-day total Antarctic accumulation and depends on the distance to the South Pole (r), the surface height (h_{sfc}) and the daily surface temperature (T_s) (Oerlemans, 2002, 2004). It therefore includes processes such as the elevation-desert effect (Pollard, 1983):

$$A = (c_a + c_b r) e^{\frac{-h_{\text{sfc}}(r)}{c_d}} e^{\kappa T_s}$$

where $c_{a,b}$ are (tuning) constants, c_d is a characteristic length scale and κ a constant describing the precipitation dependence on temperature. Only when the local temperature is below 2°C, snow is accumulated (Oerlemans, 2001).

The amount of energy available for melting (F_m) depends on the incoming energy and the thickness and heat capacity of the top surface layer (Fraedrich et al., 2005). The affected layer is 20 cm deep (d_{top}) and consists of snow (d_{snow}), soil (d_{soil}) or a mixture of both. The heat capacity (C_s) used for computation of the surface temperature is therefore computed by:

$$C_s = \frac{C_{\text{snow}} C_{\text{soil}} d_{\text{top}}}{C_{\text{snow}} d_{\text{soil}} + C_{\text{soil}} d_{\text{snow}}}$$

The atmospheric and surface temperature equations are simultaneously solved. Daily computation is necessary, because the orbital cycle as well as processes of snow accumulation and melting have a strong seasonal imprint (Pollard, 1983). The meridional heat transport (ΔF_{eo}) accounts for the coupling between the boxes, and is proportional to the temperature gradient based on the diffusion approximation (Sellers, 1970; North, 1975). The atmospheric temperatures, and also the surface temperatures, are further extrapolated towards their altitudes (h_{sfc}) according to the prescribed lapse rate, Γ_{lapse}:

$$T_a = T_a + \Gamma_{\text{lapse}} h_{\text{sfc}}(r).$$

A2 Mass balance

The mass balance is solved cumulatively on a daily basis. The specific mass balance, the total amount of accumulation or ablation (per latitude) within one year, possibly reduced by (surface or bottom) melting, evaporation or calving, is annually added to or subtracted from the snow/ice-sheet.

Table A1. List and desciption of constant parameters.

Symbol	Description	Value	Unit
ε_p	Planetary emissivity	0.61 (15° S)	–
		0.66 (45° S)	–
		0.69 (75° S)	–
ε_{11}	Emissivity constant (Sellers, 1970)	0.05	–
ε_2	Emissivity constant (Jentsch, 1987)	0.30	–
σ	Stefan-Boltzmann constant	5.67×10^{-8}	W m^{-2} K^{-4}
τ	Atmospheric transmissivity (Wang and Mysak, 2000)	0.65	–
λ	Heat exchange coefficient	10.0	W m^{-2} K^{-1}
k_1	Thermal conductance of snow	0.31	W m^{-1} K^{-1}
Δz_1	Depth range of subsurface conduction	3.0	m
ρ_{air}	Density of air	1.2	kg m^{-3}
ρ_{ice}	Density of ice	910	kg m^{-3}
ρ_w	Density of water	1000	kg m^{-3}
C_{DE}	Exchange coefficient for latent heat	1.0×10^{-3}	–
U	Wind speed	5.0	m s^{-1}
q_s^*	Sea surface specific humidity	0.8×10^{-3}	kg kg^{-1}
RH	Relative humidity (Bintanja, 1999, p. 122)	0.75	–
B_e	Equilibrium Bowen ratio	2.0	–
R_{air}	Gas constant for dry air	287.04	J kg^{-1} K^{-1} yr^{-1}
Γ_{lapse}	Atmospheric temperature lapse rate (Payne and Dongelmans, 1997)	–0.012	C m^{-1}
L_v	Latent heat of vaporation of ice	2.26×10^6	J kg^{-1}
L_m	Latent heat of melting of ice	0.334×10^6	J kg^{-1}
C_p	Specific heat capacity of dry air	1005	J kg^{-1}K^{-1}
C_{ice}	Specific heat capacity of ice	2009	J kg^{-1} K^{-1}
d_{top}	Affected snow/soil layer	0.2	m
c_a	Precipitation constant	4.44×10^{-4}	m day^{-1}
c_b	Precipitation constant	1.9569×10^{-9}	day^{-1}
c_d	Precipitation constant	3000.0	m
κ	Precipitation dependence on temperature	0.0345	K^{-1}
A_{snow}	Tangent hyperbolicus constant	50	–
B_{snow}	Tangent hyperbolicus constant	0.05	–
c_{bal}	Calving constant	–2	m yr^{-1}
α_{snow}	Albedo of snow	0.75	–
α_{ice}	Albedo of ice	0.35	–
α_{seaice}	Albedo of seaice	0.60	–
α_{land}	Albedo of land	0.30	–
α_w	Albedo of ocean water	0.10	–
x_0	Constant for sea-ice extent	2.1	–
x_1	Constant for sea-ice extent	0.6	–
T_{pd}	Temperature constant for sea-ice extent	–41	°C
C_{si}	Latitudinal shift constant for sea-ice extent	19	°

The ice sheet is allowed to grow into the surrounding ocean as long as it is hydrostatically floating. When the total weight of the ice column exceeds the floating criteria, calving occurs (Pollard, 1982) and the total mass balance (G) will be set to a negative value (c_{bal}):

$$G = c_{\text{bal}} \text{ if } \rho_{\text{air}} h_{\text{ice}} < \rho_w (h_{\text{sfc}} - h_{\text{ice}})$$

where ρ_{ice} and ρ_w are the densities of ice and water, respectively, h_{ice} is the ice thickness, and h_{sfc}, the elevation of the surface with respect to the current sea level, which is taken as a constant reference level. This crude calving parameterization also accounts for occurrence of proglacial lakes and/or marine incursions (Pollard, 1982).

Bottom melting (S) occurs when the temperature in the basal layer (T_{base}) exceeds the pressure melting point (T_{pmp}):

$$S = \frac{C_{\text{ice}}}{L_m}(T_{\text{base}} - T_{\text{pmp}})\frac{\Delta z_{\text{base}}}{\Delta t}$$

where C_{ice} is the specific heat of ice and L_m the specific latent heat of fusion of ice and Δz_{base} the thickness of the basal layer.

A3 Albedo

A separate snow balance is computed to parameterize the surface albedo. The formulas for this cumulative balance resemble the previous surface mass and energy balance equations, except for the fact that the snow depth cannot become negative. The daily derived surface albedo (α_s) depends on the snow depth (d_{snow}), when the snow layer is thicker than 10 cm:

$$\alpha = \frac{\alpha_{\text{snow}} + \alpha_{\text{ice}}}{2} + \frac{\alpha_{\text{snow}} - \alpha_{\text{ice}}}{2} \tanh(A_{\text{snow}}(d_{\text{snow}} - B_{\text{snow}}))$$

where the slope (A_{snow}) and shift (A_{snow}) are constant and α_{snow} and α_{ice} are the albedos of snow and ice, respectively. When there is less or no ice/snow, the land, ocean (low and middle latitude boxes) or sea-ice albedos (high latitude box) are used. The latitudinal extent of sea-ice (lat_{si}) is given by (Jentsch, 1987):

$$\text{lat}_{\text{si}} = \sin^{-1}[\tanh(x_0(\frac{T_{\text{pd}}}{T_a})^{x_1})] - C_{\text{si}}$$

where x_0 and x_1 are tuning constants, T_{pd} a measure for the present-day value of sea-water temperature and C_{si} a latitudinal shift.

The planetary (α_p) and atmospheric (α_a) albedos are parameterized as functions of latitude (Wang and Mysak, 2000):

$$\alpha_p = 0.6 - 0.4\cos(\text{lat})$$

$$\alpha_a = 0.3 - 0.1\sin(\text{lat}).$$

A4 Greenhouse effect

The longwave radiation constant ε_1 accounts for the greenhouse effect due to pCO_2 and other greenhouse gases:

$$\varepsilon_1 = \varepsilon_{10} + \varepsilon_{11}\sqrt{e'}$$

where, e' is the atmospheric vapor pressure, related to the saturation specific humidity (q_{sat}) and relative humidity (RH):

$$e' = 1.6 \times 10^3 \text{RH} q_{\text{sat}}$$

where:

$$q_{\text{sat}} = \frac{1.57 \times 10^{11}}{\rho_{\text{air}} R_{\text{air}} T_a} e^{\frac{-5421}{T_a}}$$

with R_{air} being the gas constant for dry air.

According to Staley and Jurica (1970) and Jentsch (1991), the CO_2-emission factor can be parameterized by:

$$\varepsilon_{10}^{CO_2} = 0.1 + 0.025\ln(CO_2). \quad \text{(A2)}$$

The other main greenhouse gas, water vapor (H_2O), also contributes about half to the (present-day) greenhouse effect. Because of the fact that we do not explicitly compute the hydrological cycle, this feedback can not be parameterized separately. To still include the effect of water vapor, we increased the climate sensitivity to pCO_2 Eq. (A2) is therefore expanded and retuned to:

$$\varepsilon_{10} = \varepsilon_{10}^{CO_2} + \varepsilon_{10}^{H_2O} = 0.27 + 0.05\ln(CO_2).$$

A doubling of atmospheric CO_2 results in a climate sensitivity of 2.5°C and modeled present-day ice-sheet size, accumulation and temperature distribution are similar to estimates (Huybrechts et al., 2000; Oerlemans, 2002).

A5 List of constant parameters

Table A1 gives an overview of the parameters used in the ice sheet-climate model.

Acknowledgements. This project was funded by the DFG (Deutsche Forschungsgemeinschaft) within the European Graduate College "Proxies in Earth History". We thank the three anonymous reviewers and the editor for their constructive comments.

Edited by: E. W. Wolff

References

Abels, H. A., Hilgen, F. J., Krijgsman, W., Kruk, R. W., Raffi, I., Turco, E., and Zachariasse, W. J.: Long-period orbital control on middle Miocene global cooling: Integrated statigraphy and astronomical tuning of the Blue Clay Formation on Malta, Paleoceanography, 20, 2362–2367, doi:10.1029/2004PA001129, 2005.

Berger, A. L.: Long Term Variations of Caloric Insolation resulting from the Earth's orbital elements, Quaternary Res., 9, 139–167, 1978a.

Berger, A. L.: Long Term Variations of Daily Insolation and Quaternary Climatic Changes, J. Atmos. Sci., 35, 2362–2367, 1978b.

Bintanja, R.: The Antarctic ice sheet and climate, Ph.D. thesis, University of Utrecht, The Netherlands, 1999.

Coxall, H. K., Wilson, P. A., Pälike, H., Lear, C., and Backman, J.: Rapid stepwise onset of Antarctic glaciation and deeper calcite compensation in the Pacific Ocean, Nature, 443, 53–57, 2005.

DeConto, R. M. and Pollard, D.: Rapid Cenozoic glaciation of Antarctica induced by declining atmospheric CO_2, Nature, 42, 245–249, 2003.

DeConto, R. M., Pollard, D., Wilson, P. A., Pälike, H., Lear, C. H., and Pagani, M.: Thresholds for Cenozoic bipolar glaciation, Nature, 455, 652–657, 2008.

Demicco, R. V., Lowenstein, T. K., and Hardie, L. A.: Atmospheric pCO_2 since 60 Ma from records of seawater pH, calcium, and primary carbonate mineralogy, Geology, 31, 793–796, 2003.

Fairbanks, R. G. and Matthews, R. K.: The Marine Oxygen Isotope Record in Pleistocene Coral, Barbados, West Indies, Quaternary Res., 10, 181–196, 1978.

Flower, B. P. and Kennett, J. P.: Middle Miocene deep-water paleoceanography in the Southwest Pacific relations with East Antarctic ice-sheet development, Paleoceanography, 10, 1095–1112, 1995.

Fraedrich, K., Jansen, H., Kirk, E., and Lunkeit, F.: The Planet Simulator: towards a user friendly model, Meteor. Zeitschrift, 14, 299–30, 2005.

Hartmann, D. L.: Global Physical Climatology, Academic Press, San Diego, 1994.

Holbourn, A., Kuhnt, W., Schulz, M., and Erlenkeuser, H.: Impacts of orbital forcing and atmospheric carbon dioxide on Miocene ice-sheet expansion, Nature, 438, 483–487, 2005.

Holbourn, A., Kuhnt, W., Schulz, M., Flores, J. A., and Anderson, N.: Orbitally-paced climate evolution during the middle Miocene "Monterey" carbon-isotope excursion, Earth Planet. Sc. Lett., 261, 534–550, 2007.

Huybers, P. and Tziperman, E.: Integrated summer insolation forcing and 40,000-year glacial cycles: The perspective from an ice-sheet/energy-balance model, Paleoceanography, 23, PA1208, doi:10.1029/2007PA001463, 2008.

Huybrechts, P.: Glaciological modelling of the Late Cenozoic East Antarctic ice sheet: Stability or dynamism?, Geogr. Ann., 75, 221–238, 1993.

Huybrechts, P.: Antarctica, in: Mass balance of the cryosphere: observations and modelling of contemporary and future changes, edited by: Bamber, J. L. and Payne, A. J., 491–523, Cambridge University Press, Cambridge, United Kingdom, 2004.

Huybrechts, P., Steinhage, D., Wilhems, F., and Bamber, J.: Balance velocities and measured properties of the Antarctic ice sheet from a new compilation of gridded data for modeling, Ann. Glaciol., 30, 52–60, 2000.

Jentsch, V.: Cloud-ice-vapor feedbacks in a global climate model, in: Irreversible Phenomena and Dynamical Systems Analysis in Geosciences, edited by: Nicolis, C. and Nicolis, G., Reidel Publishing Company, Dordrecht, The Netherlands, 1987.

Jentsch, V.: An Energy Balance Climate Model With Hydrological Cycle. 1. Model Description and Sensitivity to Internal Parameters, J. Geophys. Res., 96, 17 169–17 179, 1991.

Kürschner, W. M., Kvacek, Z., and Dilcher, D. L.: The impact of Miocene atmospheric carbon dioxide fluctuations on climate and the evolution of terrestrial ecosystems, Proc. Nat. Acad. Sci. USA, 106, 449–453, 2008.

Laskar, J., Robutel, P., Joutel, F., Gastineau, M., Correia, A. C. M., and Levrard, B.: A long-term numerical solution for the insolation quantities of the Earth, Astron. Astrophys., 428, 261–285, 2004.

Lythe, M. B., Vaughan, D. G., and the BEDMAP Consortium: BEDMAP – bed topography of the Antarctic. 1:10 000 000 scale map, British Antarctic Survey, Cambridge, United Kingdom, 2000.

Masson-Delmotte, V., Dreyfus, G., Braconnot, P., Johnsen, S., Jouzel, J., Kageyama, M., Landais, A., Loutre, M.-F., Nouet, J., Parrenin, F., Raynaud, D., Stenni, B., and Tuenter, E.: Past temperature reconstructions from deep ice cores: relevance for future climate change, Clim. Past, 2, 145–165, 2006a.

Masson-Delmotte, V., Kageyama, M., Branconnot, P., Charbit, S., Krinner, G., Ritz, C., Guilyardi, E., Jourzel, J., Abe-Ouchi, A., Crucifix, M., Gladstone, R. M., Hewitt, C. D., Kitoh, A., LeGrande, A. N., Marti, O., Merkel, U., Motoi, T., Ohgaito, R., Otto-Bliesner, B., Peltier, W. R., Ross, I., Valdes, P. J., Vettoretti, G., Weber, S. L., Wolk, F., and Yu, Y.: Past and future polar amplifications of climate change: climate model intercomparisons and ice-core constraints, Clim. Dynam., 26, 513–529, 2006b.

Miller, K. G., Mountain, G. S., Browning, J. V., Kominz, M., Sugarman, P. J., Christie-Blick, N. C., Katz, M. E., and Wright, J. D.: Cenozoic global sea level, sequences, and the New Jersey transect: results from coastal plan and continental slope drilling, Rev. Geophys., 36, 569–601, 1998.

Miller, K. G., Kominz, M., Browning, J. V., Wright, J. D., Mountain, G. S., Katz, M. E., Sugarman, P. J., Cramer, B. S., Christie-Blick, N. C., and Pekar, S. F.: The Phanerozoic record of global sea-level change, Science, 310, 1293–1298, 2005.

Myhre, G., Highwood, E. J., Shine, K. P., and Stordal, F.: New estimates of radiative forcing due to well mixed greenhouse gases, Geophys. Res. Lett., 25, 2715–2718, 1998.

North, G. R.: Theory of Energy Balance Climate Models, J. Atmos. Sci., 32, 2033–2043, 1975.

Oerlemans, J.: Glaciers and climate change, in: Modeling glacier mass balance, edited by: Oerlemans, J., chap. 4, Balkema, The Netherlands, 2001.

Oerlemans, J.: Global dynamics of the Antarctic ice sheet, Clim. Dynam., 19, 85–93, 2002.

Oerlemans, J.: Antarctic ice volume and deep-sea temperature during the last 50 Myr: a model study, Ann. Glaciol., 39, 13–19, 2004.

Pagani, M., Zachos, J. C., H., F. K., Tipple, B., and Bohaty, S.: Marked decline in atmospheric carbon dioxide concentrations during the Paleogene, Science, 309, 600–603, 2005.

Payne, A. J. and Dongelmans, P. W.: Self-organization on the thermomechanical flow of ice sheets, J. Geophys. Res., 106, 12219–12233, 1997.

Pearson, P. N. and Palmer, M. R.: Atmospheric carbon dioxide concentrations over the past 60 million years, Nature, 406, 695–699, 2000.

Pekar, S. F. and DeConto, R. M.: High-resolution ice-volume estimates for the early Miocene: Evidence for a dynamic ice sheet in Antarctica, Palaeogeogr. Palaeocl., 231, 101–109, 2006.

Pollard, D.: A simple ice sheet model yields realistic 100 kyr glacial cycles, Nature, 296, 334–338, 1982.

Pollard, D.: A Coupled Climate-Ice Sheet Model Applied to the Quaternary Ice Ages, J. Geophys. Res., 88, 7705–7718, 1983.

Pollard, D. and DeConto, R. M.: Hysteresis in Cenozoic Antarctic ice-sheet variations, Global Planet. Change, 45, 9–21, 2005.

Randall, D. A., Wood, R. A., Bony, S., Colman, R., Fichefet, T., Fyfe, J., Kattsov, V., Pitman, A., Shukla, J., Srinivasan, J., Stouffer, R., Sumi, A., and Taylor, K.: Climate Change 2007: The Scientific Basis, Contribution of Working Group 1 to the Fourth Assessment Report of the Intergovernmental Panel on Climate Change, edited by: Solomon, S., Qin, D., Manning, M., Chen, Z., Marquis, M., Averyt, K., Tignor, M., and Miller, H., p. 881, Cambridge University Press, Cambridge, United Kingdom and New York, NY, USA, 2007.

Raymo, M. E.: The initiation of northern hemisphere glaciation, Paleoceanography, 9, 399–404, 1994.

Raymo, M. E. and Niscancioglu, K.: The 41 kyr world: Milankovitch's other unsolved mystery, Paleoceanography, 18, 1011, doi:10.1029/2002PA000791, 2003.

Schrag, D. P., Hampt, G., and Murray, D. W.: Pore fluid con-

straints on the temperature and oxygen isotopic composition of the Glacial Ocean, Science, 272, 1930–1932, 1996.

Sellers, W. D.: A global climate model based on the energy balance of the earth-atmosphere system, J. Appl. Meteorol., 8, 392–400, 1970.

Shevenell, A., Kenneth, J. P., and Lea, D. W.: Middle Miocene Southern Ocean cooling and Antarctic cryosphere expansion, Science, 305, 1766–1770, 2004.

Shevenell, A., Kenneth, J. P., and Lea, D. W.: Middle Miocene ice sheet dynamics, deep-sea temperatures, and carbon cycling: A Southern Ocean perspective, Geochem. Geophy. Geosy., 9, Q02006, doi:10.1029/2007GC001736, 2008.

Sima, A.: Modeling oxygen isotopes in ice sheets linked to Quaternary ice-volume variations, Ph.D. thesis, University of Bremen, Germany, 2005.

Sima, A., Paul, A., Schulz, M., and Oerlemans, J.: Modeling the oxygen-isotope composition of the North American Ice Sheet and its effect on the isotopic composition of the ocean during the last glacial cycle, Geophys. Res. Lett., 33, L15706, doi: 10.1029/2006GL026923, 2006.

Staley, D. O. and Jurica, G. M.: Flux emissivity tables for water vapor carbon dioxide and ozone, J. Appl. Meteorol., 9, 365–372, 1970.

Van Tuyll, C. I., van de Wal, R. S. W., and Oerlemans, J.: The response of a simple Antarctic ice-flow model to temperature and sea-level fluctuations over the Cenozoic era, Ann. Glaciol., 46, 69–77, 2007.

Wang, Z. and Mysak, L. A.: A simple coupled atmosphere-ocean-sea ice-land surface model for climate and paleoclimate studies, J. Climate, 13, 1150–1172, 2000.

Zachos, J. C., Pagani, M., Sloan, L., Thomas, E., and Billups, K.: Trends, Rythms, and Aberrations in Global Climate 65 Ma to Present, Science, 292, 686–693, 2001.

Zachos, J. C., Dickens, G. R., and Zeebe, R. E.: An early Cenozoic perspective on greenhouse warming and carbon-cycle dynamics, Nature, 451, 279–283, 2008.